Journal of Science and Transport Technology
Journal homepage: https://jstt.vn/index.php/en

Numerical analysis of aerodynamic and structure characteristics of an autonomous unmanned flying car for high-rise building rescue operations in urban area

Cong-Thanh Nguyen[1], Hoang-Quan Chu[2], Thai-Son Vu[1], Xuan-Truong Le[1], Cong-Truong Dinh[1,*]

[1]School of Mechanical Engineering, Hanoi University of Science and Technology, No 1 Dai Co Viet St. Hai Ba Trung Dist., Hanoi 11615, Vietnam

[2]Faculty of Aerospace Engineering, Le Quy Don Technical University, No. 236 Hoang Quoc Viet St., Bac Tu Liem Dist., Hanoi 11917, Vietnam

Article info
Type of article:
Original research paper

DOI:
https://doi.org/10.58845/jstt.utt.2023.en.3.4.1-9

***Corresponding author:**
E-mail address:
truong.dinhcong@hust.edu.vn

Received: 02/09/2023
Revised: 20/11/2023
Accepted: 22/11/2023

Abstract: Using numerical commercial software, this article presents a type of autonomous unmanned flying car capable of saving people in burning high-rise buildings in urban areas. This kind of flying vehicle is maneuverable and fast, and it has the ability to anchor to the building balconies to receive people in distress. Initial, a computational simulation is performed to investigate the aerodynamic properties of the propeller without and with a guard ring. A full-scale model evaluation based on Buckingham-Pi theory is then performed to evaluate the aerodynamic and structural characteristics of the proposal. Numerical simulation results show that the proposed design is feasible.

Keywords: ANSYS, Flying car, Rescue operations, Aerodynamic, Structure.

1. Introduction

Nowadays, urbanization and population growth speed are increasing rapidly around the world. This leads to numerous problems regarding conventional transportation infrastructures and vehicles, notably congestion [1]. Thus, flying cars come into the prospect as an alternative to traditional automobiles. Most flying car designs up to date are based on the quadcopter configuration, commonly found in unmanned drones. This is because quadcopters have very high mobility. They can take off and land vertically at high speed and in small spaces. Therefore, quadcopters, or unmanned drones in general can be used as a means to conduct search and rescue operations [2]. On the other way, saving victims from dangerous situations can be done quickly thanks to flying cameras.

In fact, the idea is to implement a flying car with the capability to carry passengers to conduct rescue operations, ideally in tall buildings. In the case of a fire in the high level of a building and the victim is trapped, the vehicle can be dispatched, rapidly to the level of the incident, and people can enter and descend to ground level unharmed. This helps the process to become much earlier and thus ensures the safety of the victim. The aspect of this design is very promising as more and more tall building continues to rise in major cities in Vietnam [3].

2. Experimental Setup

2.1. Propeller Description

Figure 1 illustrates a propeller HQ 8x4x3 Prop, which is rotated by an electric motor XING2 3106 FPV Motor Unibell, is provided by the same company iFlight FPV [4, 5]. This propeller having 3

blades, 8-inch diameter (203.2 mm), and a pitch angle of 4° produces thrust force, which is measured with each corresponding throttle level. In this case, the throttle input signal is provided by the Frsky Taranis X9D Plus 2019 radio transmitter as PWM pulse vary from 1000 μs being zero throttle to 2000 μs being maximum [6].

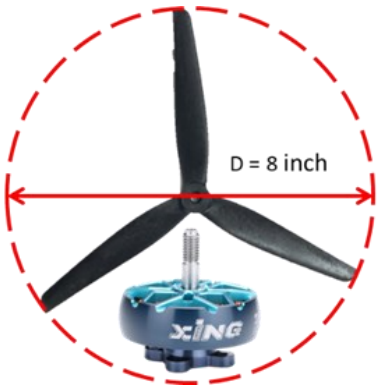

Fig. 1. Propeller and electric motor

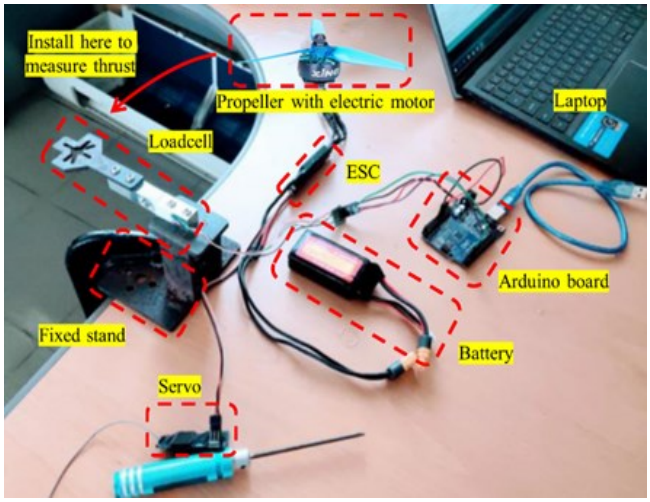

Fig. 2. Test bench setup

Table 1. Experimental results of the propeller

Throttle (μs)	RPM	Thrust (No guard) (kg)
1100	3614	0.08
1200	6085	0.25
1300	8928	0.53
1400	11128	0.86
1500	13147	1.19
1600	14985	1.53
1700	17042	1.79
1800	17528	1.85
1900	18557	2.01
2000	19085	2.13

2.2. Thrust Measurement

Figure 2 displays an experimental setup measure propeller thrust at Propulsion Systems Laboratory, Hanoi University of Science and Technology. Battery, ESC, and servo are connected to a propeller with electric motor like controlling a regular drone. A loadcell that is fixed on a test stand to place the propeller is combined with an Arduino board to measure propeller thrust. Finally, the display of results through Arduino IDE coding software on the computer. The results obtained are presented in Tab.1.

Table 2. Parameters for the prototype model

Parameter	Value
Dimensions	744 x 524 x 368 mm
Total weight	2.5 kg
Max payload	1 kg

3. Numerical Analysis

3.1. Model Design Description

When designing a UAV, the most important factor that comes to mind is the maximum payload that it can carry. Research is considered in Vietnam, where the average weights of Vietnamese men and women for the age from 45 to 54 are 61.1 kg and 55.4 kg, respectively [7]. Thus, it is decided that 120 kg is the maximum value that the craft can carry. Therefore, the vehicle is capable of carrying one adult passenger with safety. The factor of safety needs to be reflected as well. According to reference [8], the chosen safety factor is 1.5. With the vehicle being used for rescue operations, the safety factor will be 1.6 to ensure total safety for the passengers. According to the estimated max take-off weight is around 200kg, therefore the max thrusts needed will be 400 kg.

The maximum altitude that the craft can reach is 500m, which allows it to reach an 80-store tall building. In many cases, this ensures the vehicle can access traditional apartments with 20 or 30 levels. Flight time is around 15 to 20 minutes for any operations to go smoothly. This is important when comes to choosing the right battery and propulsion systems.

For the craft to be able to carry out its missions, a docking mechanism is required for the attachment to the balcony of any apartment. The craft can stay stationary during the dock for the passenger to come in. Grippers with pneumatic actuators are taken into consideration for their strength while being lighter than hydraulics. Besides that, the side of the craft can act as a platform for the passenger to step in.

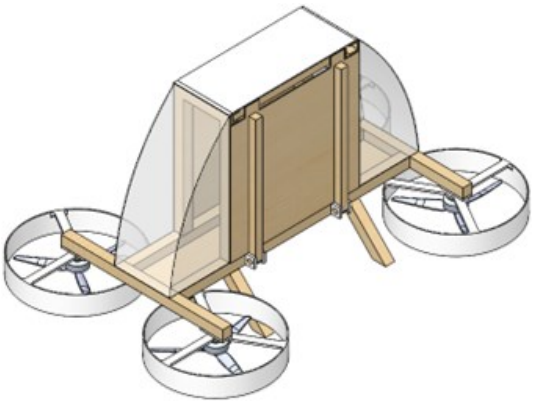

(a) Flying car prototype

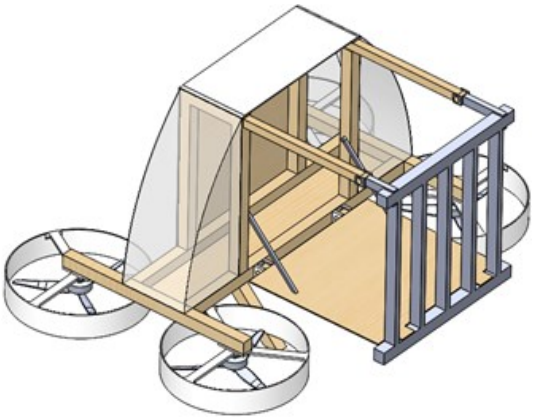

(b) Docking mechanism

Fig. 3. Prototype model with docking mechanism

For the materials, carbon fiber is a well-known element in UAV fabrication with its outstanding properties of lightweight and high durability [9]. However, with the restriction of high prices, for creating a small version of the model, the frame material is resolved to pine wood, which is also lightweight in combination with high stiffness, though slightly heavier. Its performance is suitable for frame construction [10].

To perform simulations and experimental validations of the design, the creation of a scale model is needed as it is easier to perform, saving money and resources. The model is a quadcopter with an H-frame configuration (Fig. 3a). The H-frame along with the X-frame are the most common configurations used for this type of aircraft. The reason the H-frame was chosen is that it had a stretched rectangular structure, which can accommodate a lot of space in the middle for the payload, as well as any electronic components and batteries [11]. The structure of the frame is also very simple with only four beams, making it very lightweight. The inspiration for the design is loosely based on the Jetson One, the first affordable personal eVTOL on the market [12]. The parameters for the research prototype model as shown in Tab.2. The gripper arms and the side plate will have servo as actuators for quick action and lightweight (Fig. 3b).

3.2. Fundamental Theory

To validate the design concept via a prototype model, Buckingham Pi theorem is used to create a dynamic similitude between the two of them, by creating dimensionless ratios known as Pi group. Coutinho et al had made a review on the subject and its application in engineering [13]. Hoblet et al. had used the theorem to develop a scale model car for the design of a steering controller to implement into real vehicle [14]. Veeranjaneyulu et al had also applied the theorem in their design of an aerial hoverboard [15]. In this article, the Pi groups are created by identifying key dimensional physical parameter than applying dimension analysis to form the dimensionless ratios. In our case, the following are required: Air density (ρ), Angular velocity of the propeller (ω), Gravitational acceleration (g), Maximum thrust (T), Rotor diameter (d), and Total weight (m). These are the basic parameters for analyzing the dynamics of a quadcopter based on helicopter aerodynamics [16]. From this parameters, three dimensionless Pi groups are form:

$$\Pi_1 = \frac{T}{\rho d^4 \omega^2}; \Pi_2 = \frac{m}{\rho d^3}; \Pi_3 = \frac{gd}{\omega^2} \quad (1)$$

The first Pi group illustrates the relation of thrust, the second one being for weight and the third one for gravitational force. With this, relation is established between the two models. To create a full-scale vehicle that is dynamically like the prototype, the Pi groups of the two must equal. From this, we can perform experimental research on the prototype model and optimize the design of the full-scale version.

4. Results and Discussion

4.1. Grid Dependency Test

In the present study, the governing differential equations, including continuity, Reynolds-averaged Navier-Stokes (RANS), and energy equations, are solved numerically to study the flow characteristics of the model [17-21]. The simulations are conducted using the commercial software ANSYS Fluent 19.1 [22].

As remarked above, the propeller used for the flying car sub-scale model is the HQ 8x4.5x3 with diameter D = 8 inch (203.2 mm). For geometry conditions, the rotating domain of the propeller has diameter of 1.04D, heigh of 0.4D. The optimal value of those is 1.1D and 0.4D according to Kutty and Rajendran [23] but we reduce it because the drone has a propguard with 1.1D in diameter and 40 mm in height. For this analysis, the propguard is not required. The static domain is a cylinder of 10D in diameter and 10D in height (Fig. 4a).

For the best results, it is necessary to assess which turbulence model is the best for the problem. Simulations will be performed with the Spalart-Allmaras (S-A), k-epsilon (k-ε) and SST k-omega (SST k-ω) model on a single propeller. The result is validated with the experimental test bench results (Tab.1) as done in “Experimental setup” part.

The mesh is performed using the tetrahedrons method (Fig. 4b). A 10 layers inflation is put at the surface of the propeller with the 1st layer thickness at 0.02 mm and a growth rate of 1.2. With this setup, the value of y^+ number is 0.73.

The results illustrate that the difference between the thrust values is insignificant (Fig. 5). The S-A has a 5% higher value than the ones of the other twos. The difference between k-ε and SST k- ω is roughly 2%. Both of this model have a 6% decrease compared to the experiment results. Due to the nature of the problem, accurate analysis is needed in near wall regions such as propeller or the model cover surface, the SST k- ω is chosen for the entire CFD analysis.

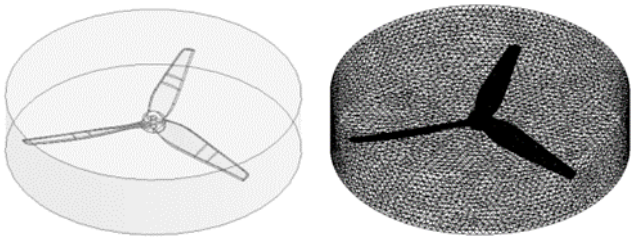

(a) Geometry (b) Meshing

Fig. 4. Rotating domain without propguard.

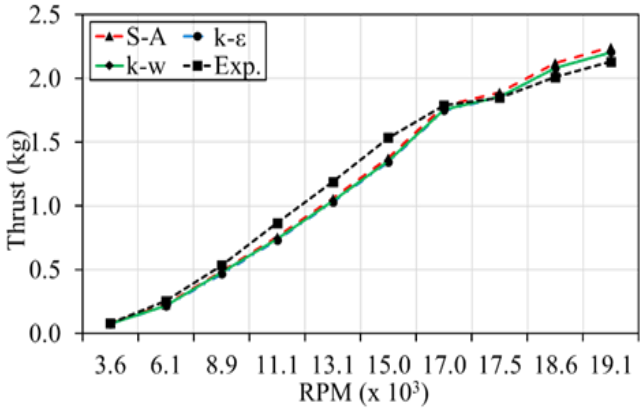

Fig. 5. Numerical and experimental results.

4.2. Propeller Analysis

With the design having a propeller guard (Fig. 6a), it is necessary to assess its affect to the performance of the propeller in terms of generated thrust to validate the flying capability of the model. The mesh generation and boundary conditions are the same as the no guard simulation (Tab. 3).

The guarded propeller mesh is illustrated in Fig. 6b. The thrust results (Fig. 7) can be seen from the graph. It is easy to notice that there are some noticeable differences in the results. There is a 10% difference between the values of the open propeller simulation to those of the test. Besides that, there is also a 10% drop in force in the case of propeller guard compared to open propeller. This is acceptable as guard is mainly for protection

purposes and the generated force is still sufficient for take-off. The craft with the maximum take-off weight of 3.5 kg will be able to operate at a throttle level of 50% to 60% with the thrust of 1 kg per propeller, leading up to 4 kg total.

The velocity and pressure contours show the values distributed around the propeller blade area (Fig.8-9). While high velocity values are concentrated in the blade tip region, in the propeller hub is the low velocity area (Fig.8). The airflow passing through the propeller zone is accelerated to about 50-60 m/s (i.e., the white area just below the rotating zone). There is a small sector of high pressure at the blade leading edge and a large zone of low pressure on the blade suction side (Fig.9). This pressure difference explains why the blades create thrust. These results are in perfect agreement with the basics of aerodynamics.

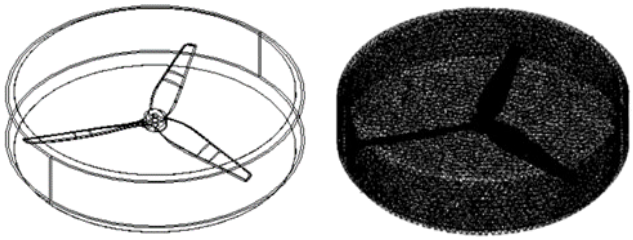

(a) Geometry (b) Meshing

Fig. 6. Rotating domain with prop guard

Table 3. Mesh statistics of two simulation models

Mesh statistics	Nodes	Elements
No guard	190,960	691,734
With guard	224,619	869,277

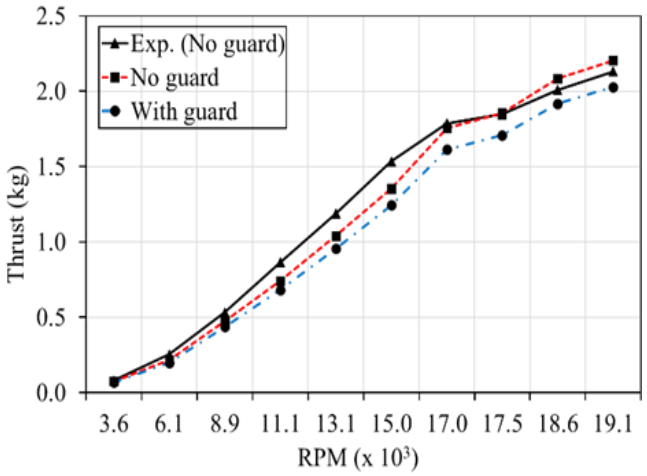

Fig. 7. Thrust relation to the RPM of the motor.

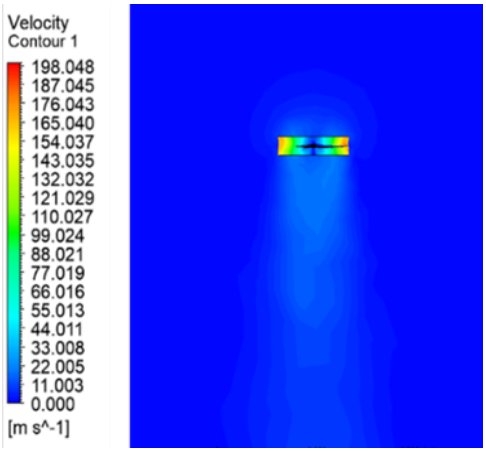

Fig.8. Velocity contour of the domain

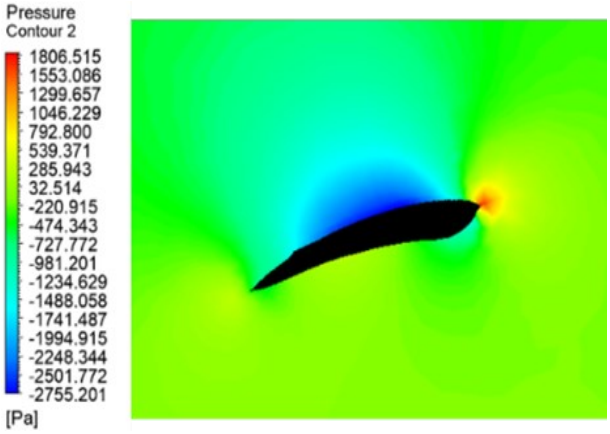

Fig. 9. Pressure contour at 50% radius

4.3. Full Model Simulations

With the propeller fully capable to lift the UAV, the entire body simulations are conducted to validate the design aerodynamic, so that improvement can be made to the model. The static domain dimension is set to ensure that the distance between the model and the ground is greater than 5D to avoid ground effect (Fig.10a). All the mesh setup is identical to those for the propellers (Fig.10b). The inlet velocity is 5 m/s, and the propellers will be spinning at 14,987 RPM, which is equivalent to 50% throttle.

The pressure on the body is mainly focus on the roof at 18.18 Pa (Fig.11a). In addition, the simulation results show that there are some vortices that formed under the body (Fig.11b). This is a major factor that contribute to the drag and optimization is needed. The propeller generates an 8.8 N of force individually, creating a total thrust of 35.2 N, which is sufficient for operation. Moreover,

the drag force on the body is 3.8 N (11% of the thrust). The body shape can be further optimized to reduce the number. All in all, the model can perform normally flying vertically at 5 m/s (Fig.12).

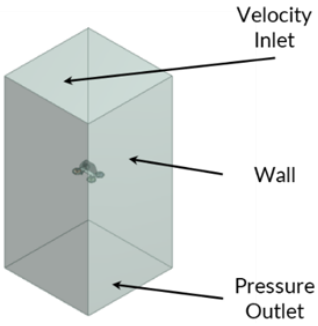

(a) Boundary conditions

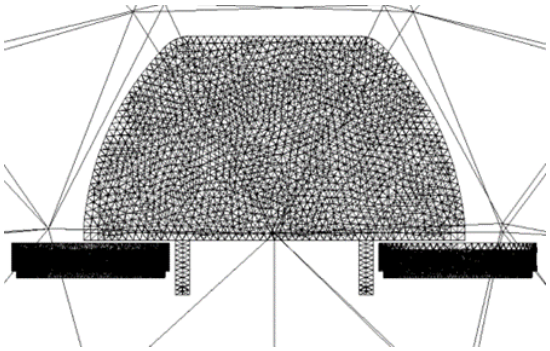

(b) Meshing on the body

Fig. 10. Full model boundary conditions, meshing

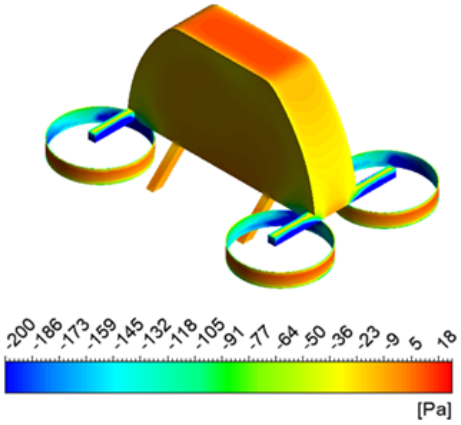

(a) Pressure contour on the body

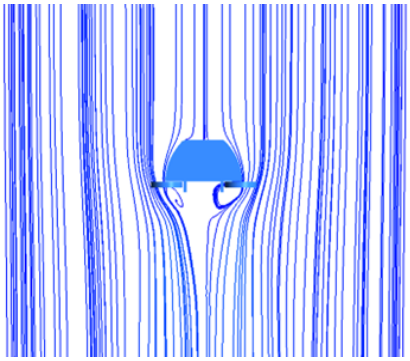

(b) Streamline through the body

Fig. 11. Streamline and contour on the body

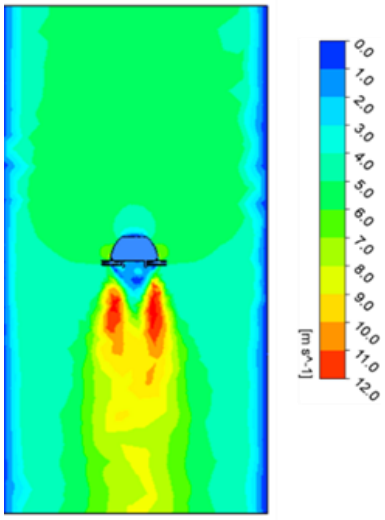

Fig. 12. Velocity contour of the full model

4.4. Structure Simulation

This is an important step to validate the structural strength of the docking mechanism to see whether it can meet the requirements. The model, as shown in Fig. 13, is simplifying with only the frame structure being the target for simulation. Important values that need to be obtain are the equivalent stress and the total deformation of the structure [24-26].

The mesh is achieve using hex dominant method (Fig. 14). The material for the frame is pine wood, which has a density of 487 kg/m^3 and the ultimate strength of 66.3 MPa. The Young's Modulus and the Poisson ratio for the wood are 9300 MPa and 0.374, respectively. For boundary conditions, fixed support will be set at the gripper contact surface and the bridge platform. A force distribution of 10 N is put on to the middle plate to represents the maximum payload that the craft is allowed to carry along with 25N of gravitational force on the weight of the craft (Fig. 15).

From the results, the total deformation of the frame at docking is very small compared to the aircraft dimensions (Fig. 16). The stress on the frame is also actual insignificant in comparison to the ultimate strength (Fig. 17a). The high stresses, as shown in Fig. 17b, are focused in the linkage area between the beam and the gripper at about

14.3 Pa (22% of the ultimate strength).

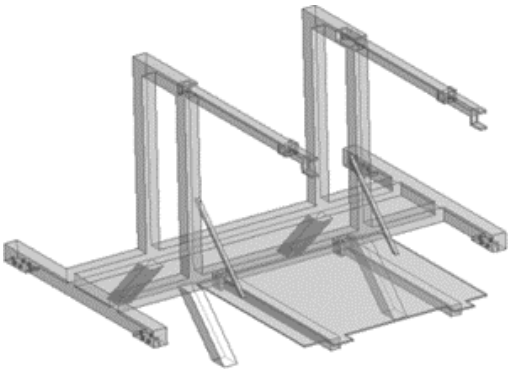

Fig. 13. Bridge platform structure

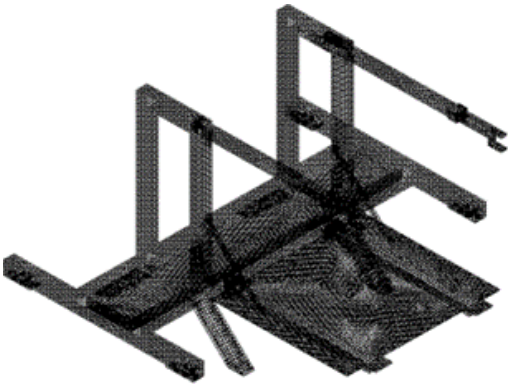

Fig. 14. Structural meshing of the model

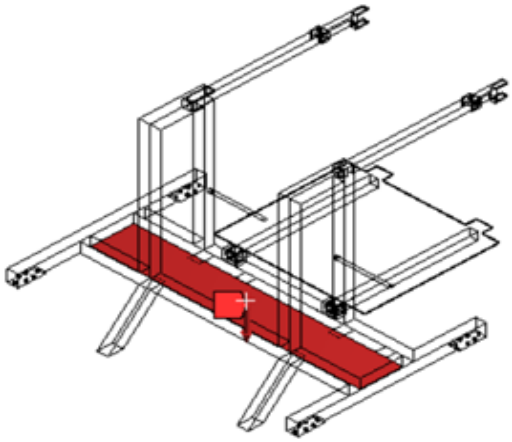

Fig. 15. Location of the force on the model

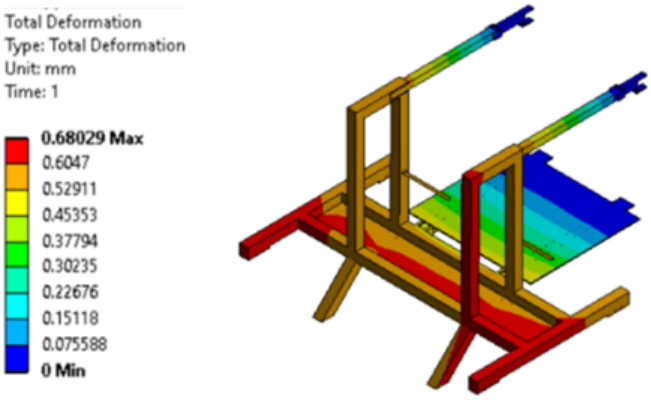

Fig. 16. Total deformation

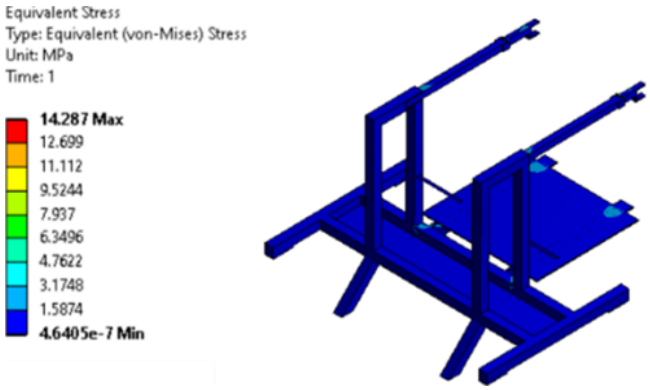

(a) Full body stress

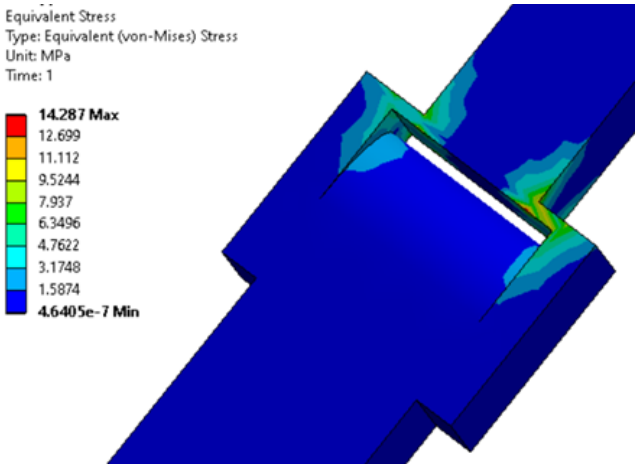

(b) Linkage between the arm and the gripper

Fig. 17. Equivalent stress on the model

5. Conclusions

To summarize, from the simulation, the prototype model has the capability to operate normally and meets all the requirements. The model can operate safely at around 50 % of is power potential, providing 4 kg of total thrust which satisfy the safety factor of 2.as the maximum payload allowed is 1 kg. The design still needs to be improved and further optimized for better aerodynamic performance, most notably being the optimization of the propeller guard design for optimizing thrust.

Besides that, weight optimization will also need to consider. The docking mechanism will also be improved on the structural aspect. All the test results on the model obtained in future research will be used to optimize the design parameters of the full-scale vehicle. The next goal of the research is to develop the scale model and conduct experimental analysis for validation purposes.

Acknowledgments

This research work is funded by Ministry of Education and Training, Vietnam under grant number B2023-BKA-11.

References

[1]. G. Pan and M.S. Alouini. (2021). Flying Car Transportation System: Advances, Techniques, and Challenges. *IEEE Access*, 9, 24586-24603.

[2]. J.N. McRae, C.J. Gay, B.M. Nielsen, and A.P. Hunt. (2019). Using an Unmanned Aircraft System (Drone) to Conduct a Complex High-Altitude Search and Rescue Operation: A Case Study. *Wilderness & Environmental Medicine*, 30(3), 287-290.

[3]. Council on Tall Buildings and Urban Habitat. (2023). The 100 tallest completed buildings in Vietnam in 2023. Available at: https://www.skyscra%er.com/buildings.

[4]. iFlight FPV. (2023). HQ 8x4x3 Prop. Available at: https://shop.iflight-rc.com/hq-8x4x3-cw-ccw-propeller-4pcs-2pirs-pro1547.

[5]. iFlight FPV. (2023). XING2 3106 FPV Motor Unibell. Available at: https://shop.iflight-rc.com/xing2-3106-fpv-motor-unibell-pro1476.

[6]. Frsky. (2019). Instruction Manual for FrSky Taranis X9D Plus/SE 2019. *FrSky Electronic Co., Ltd.*

[7]. L. Helen, M.P.H. Walls, A. Peeters, T.S. Pham, N.Q. Nguyen, T.T.H Nguyen, D.L. Do, L.V. Nguyen, G.K. Pham, M.R. Christopher. (2009). Prevalence of underweight, overweight and obesity in urban Hanoi, Vietnam. *Asia Pac J Clin Nutr* 2009,18 (2), 234-239.

[8]. J.Z. John, M.J. Thomas, and E.L. Curtis. (2016). The Ultimate Factor of Safety for Aircraft and Spacecraft - Its History, Applications and Misconceptions. *AIAA/ASCE/AHS/ASC Structures, Structural Dynamics, and Materials Conference. NASA*. USA. Available at: https://ntrs.nasa.gov/citations/20150003482.

[9]. R. Mirski, D. Dziurka, M. Chuda-Kowalska, M. Wieruszewski, J. Kawalerczyk and A. Trociński. (2020). The Usefulness of Pine Timber (Pinus sylvestris L.) for the Production of Structural Elements. Part I: Evaluation of the Quality of the Pine Timber in the Bending Test. *Materials*, 13(18), 3957.

[10] M.M. ElFaham, A.M. Mostafa, and G.M. Nasr. (2020). Unmanned aerial vehicle manufacturing materials: Synthesis, spectroscopic characterization and dynamic mechanical analysis. *Journal of Molecular Structure*, 1201, 127211.

[11]. K.R. Dixit, P.P. Krishna and R. Antony. (2017). Design and development of H frame quadcopter for control system with obstacle detection using ultrasound sensors. *IEEE Xplore*. Available at: https://ieeexplore.ieee.org/document/8394166.

[12]. G. Gorant. (2021). This New One-Person eVTOL Is Like a Real-Life 'Star Wars' Landspeeder. Robb Repport. Penske Media Corporation. *WordPress.com*. Available at: https://robbreport.com/motors/aviation/jetson-one-evtol-1234643732/.

[13]. C.P. Coutinho, A.J. Baptista, and J.D. Rodrigues. (2016). Reduced scale models based on similitude theory: A review up to 2015. *Engineering Structures*, 119, 81–94.

[14]. P.C. Hoblet, R.T. O'Brien, and J.A. Piepmeier. (2003). Scale-model vehicle analysis for the design of a steering controller. *Institute of Electrical and Electronics Engineers (IEEE)*, 309.

[15]. K. Veeranjaneyulu, V. Gnan, K.S. Kiran, G. Sravanthi, and A.U. Deepika. (2023). Similitude analysis and model fabrication of aerial hoverboard. *AIP Conference Proceedings*, 2492(1), 020083.

[16]. J.G. Leishman. (2006). Principles of helicopter aerodynamics. *Cambridge University Press*. UK.

[17]. T.L. Nha, V.H. Nguyen, X.T. Le, and C.T. Dinh. (2023). Aerodynamic Performance of Single-Stage Transonic Axial Compressor with Multi-

Bleed Airflow. *Proceedings of the 3rd Annual International Conference on Material, Machines and Methods for Sustainable Development (MMMS2022)*. *Lecture Notes in Mechanical Engineering (LNME)*, pp 109-116. Springer, Cham.

[18]. D.Q. Tran, V.H. Nguyen, T.S. Vu, C.T. Dinh, T.C. Nguyen, and X.L. Bui. (2023). Aerodynamic Performance of a Single-stage Transonic Axial Compressor using a Hybrid Inclined Groove-Recirculation Casing Treatment. *Journal of Aeronautics, Astronautics and Aviation*, 55(2), 143-158.

[19]. H.Q. Chu, Q.H. Nguyen, Q.H. Nguyen, Q.V. Nguyen, V.H. Nguyen, T.K.D. Hoang, X.T. Le, C.T. Dinh, and T.T. Tran. (2022). Aerodynamic Performance of a Multi-stage Axial Compressor with Tip Clearance Coupled with Hub Fillet. *The AUN/SEED-Net Joint Regional Conference in Transportation, Energy, and Mechanical Manufacturing Engineering (RCTEMME 2021). Lecture Notes in Mechanical Engineering. Springer Nature Singapore*, pp 1306-1323.

[20]. D.Q. Tran, X.T. Le, V.H. Nguyen, C.T. Dinh, T.S. Vu. (2022). Aerodynamic Performance Optimization of a Single-stage Axial Compressor using Circumferential Bleeding Airflow. *Journal of Aeronautics, Astronautics and Aviation*, 54(4), 451-466.

[21]. A.T. Nguyen, D.H. Vo, C.T. Dinh, and H.Q. Chu. (2022). Aerodynamic performances of a single-stage transonic axial compressor using an inclined casing groove. *Australian Journal of Mechanical Engineering,* 22(1), 179-188

[22]. ANSYS. (2018). ANSYS Fluent Theory Guide. ANSYS 19.1, *ANSYS Inc*, USA.

[23]. H. Kutty and P. Rajendran. (2017). 3D CFD Simulation and Experimental Validation of Small APC Slow Flyer Propeller Blade. *Aerospace*, 4(1), 10.

[24]. H.Q. Chu, and C.T. Dinh. (2023). Aerodynamic and structural performances of a single-stage transonic axial compressor with blade fillet radius. *International Journal of Intelligent Unmanned Systems*, 11(3), 407-424.

[25]. C.T. Dinh, T.D. Vuong, X.T. Le, T.M. Nguyen, and Q.H. Nguyen. (2020). Aeromechanic performance of a single-stage transonic axial compressor with recirculation-bleeding channels. *Australian Journal of Mechanical Engineering*, 21(1), 154-167.

[26]. C.T. Dinh, D.Q. Vu and K.Y. Kim. (2020). Effects of Rotor-Bleeding Airflow on Aerodynamic and Structural Performances of a Single-Stage Transonic Axial Compressor. *International Journal of Aeronautical and Space Sciences*, 21, 599-611.